

## RESEARCH ARTICLE

[View Article Online](#)  
[View Journal](#) | [View Issue](#)

 Cite this: *Inorg. Chem. Front.*, 2024,  
 11, 3150

# Discovery of excellent ultraviolet nonlinear optical materials in chlorates and bromates with highly stereochemically active lone pairs†

 Chun-Li Hu,<sup>a,b</sup> Qian-Qian Chen,<sup>b</sup> Fang Kong <sup>b</sup> and Jiang-Gao Mao <sup>\*a,b</sup>

The discovery of short-wave ultraviolet (SWUV,  $\lambda_{PM} < 266$  nm, PM = phase-matching) and deep ultraviolet (DUV,  $\lambda_{PM} < 200$  nm) nonlinear optical (NLO) crystals is urgently required and full of challenges. Unlike the conventional strategy of using  $\pi$ -conjugated groups (such as  $\text{BO}_3$ ) as core motifs for constructing UV NLO crystals, herein the long-neglected stereochemically active lone pair (SCALP) groups  $\text{ClO}_3$  and  $\text{BrO}_3$  are innovatively proposed to be good UV NLO functional motifs based on the group property prediction, and the NLO performance of chlorates and bromates has been investigated systematically for the first time by first-principles methods. Benefiting from the high polarizability of  $\text{ClO}_3$  and  $\text{BrO}_3$  and their favorable alignments, the halate crystals  $\text{AClO}_3$  and  $\text{ABrO}_3$  ( $A = \text{NH}_4, \text{K}, \text{Rb}$  and  $\text{Cs}$ ) exhibit high SHG coefficients comparable to that of classical  $\beta\text{-BaB}_2\text{O}_4$  ( $4.2\text{--}4.8 \times \text{KDP}$  for  $\text{AClO}_3$  and  $6.1\text{--}7.1 \times \text{KDP}$  for  $\text{ABrO}_3$ ). Meanwhile, their wide band gaps and large optical anisotropy lead to very short  $\lambda_{PM}$  deep into DUV and SWUV (185–195 nm for  $\text{AClO}_3$  and 210–220 nm for  $\text{ABrO}_3$ ). Remarkably,  $\text{ABrO}_3$  shows a rare full-wave-length phase-matching capability. Hence  $\text{AClO}_3$  and  $\text{ABrO}_3$  could be promising DUV and SWUV NLO candidates, respectively, and the UV NLO potential of  $\text{ClO}_3$  and  $\text{BrO}_3$  is further demonstrated by profound mechanism analysis. This work opens up a new avenue for the development of SWUV and even DUV NLO materials.

 Received 20th February 2024,  
 Accepted 26th March 2024

DOI: 10.1039/d4qi00462k

[rsc.li/frontiers-inorganic](https://rsc.li/frontiers-inorganic)

## Introduction

As vital optoelectronic functional materials, nonlinear optical (NLO) crystals can extend limited and fixed laser wavelengths to the ultraviolet and infrared spectral ranges through various kinds of frequency conversion techniques, such as second harmonic generation (SHG), *etc.* Due to their wide applications in many important fields, such as ultrahigh-resolution laser lithography, biomedicine and high-precision scientific instruments, short-wave ultraviolet (SWUV,  $\lambda_{PM} < 266$  nm, PM = phase-matching) and deep ultraviolet (DUV,  $\lambda_{PM} < 200$  nm) NLO crystals have attracted ever-growing attention from chemists and materials scientists.<sup>1–5</sup>

The indispensable prerequisite for being an NLO crystal is the noncentrosymmetric structure constructed by NLO functional motifs.<sup>6,7</sup> Over the past decades, several important NLO-active motifs with wide UV transmittance windows, including

the  $\pi$ -conjugated  $\text{BO}_3$ ,  $\text{CO}_3$  and  $\text{C}(\text{NH}_2)_3$  planar triangles and the  $\sigma$ -bonded  $\text{BO}_n\text{F}_{4-n}$  and  $\text{PO}_n\text{F}_{4-n}$  tetrahedra, have been frequently involved in the exploration of UV NLO materials and some potential SWUV and DUV NLO borates, carbonates, guanidinium salts and phosphates have been developed, including the notable  $\beta\text{-BaB}_2\text{O}_4$  ( $\beta\text{-BBO}$ ) and  $\text{KBe}_2\text{BO}_3\text{F}_2$  (KBBF), as well as the newly discovered  $\text{CsB}_4\text{O}_6\text{F}$ ,  $\text{C}(\text{NH}_2)_3\text{BF}_4$ ,  $\text{ABC}_3\text{F}$ ,  $\text{NaNH}_4\text{PO}_3\text{F}\cdot\text{H}_2\text{O}$ , *etc.*<sup>8–12</sup>

The stereochemically active lone pair (SCALP) groups, represented by  $\text{IO}_3$ ,  $\text{SeO}_3$  and  $\text{TeO}_3$ , exhibit their natural advantages in the nonlinear optical field because the SCALP electrons can induce cations ( $\text{I}^{5+}$ ,  $\text{Se}^{4+}$  and  $\text{Te}^{4+}$ ) to undergo second-order Jahn–Teller (SOJT) distortion and endow the groups with large hyperpolarizability and polarizability anisotropy.<sup>13,14</sup> In recent years, numerous excellent NLO crystals with such groups have been discovered, such as  $\text{AlO}_3$  ( $A = \text{Li}, \text{Rb}, \text{Cs}$ ),  $\text{Li}_2\text{M}(\text{IO}_3)_6$  ( $M = \text{Ge}, \text{Sn}, \text{Ti}$ ),  $\text{BiFSeO}_3$ ,  $\text{Pb}_2\text{Bi}(\text{SeO}_3)_2\text{Cl}_3$ ,  $\text{TlSb}_3\text{Te}_2\text{O}_{12}$ , *etc.*<sup>15–23</sup> They are mostly only used in the IR NLO field due to their relatively small band gaps. Therefore, the SCALP groups are generally considered to be the IR NLO-active motifs rather than the UV ones. However, our calculations have revealed that other less-common SCALP groups have the potential to be excellent UV NLO-active motifs.

The elements chlorine and bromine are located in the same main group as iodine in the periodic table and have the penta-

<sup>a</sup>Fujian Science & Technology Innovation Laboratory for Optoelectronic Information of China, Fuzhou, Fujian 350108, P. R. China. E-mail: [mjg@fjirsm.ac.cn](mailto:mjg@fjirsm.ac.cn)

<sup>b</sup>State Key Laboratory of Structural Chemistry, Fujian Institute of Research on the Structure of Matter, Chinese Academy of Sciences, Fuzhou 350002, P. R. China

†Electronic supplementary information (ESI) available: Calculated band structures, refractive index curves and the electron localization function. See DOI:

<https://doi.org/10.1039/d4qi00462k>

valent ionic forms with  $\text{Cl}^{5+}\text{-}3s^2$  and  $\text{Br}^{5+}\text{-}4s^2$  SCALP electrons. Like  $\text{I}^{5+}$  in iodates,  $\text{Cl}^{5+}$  and  $\text{Br}^{5+}$  are commonly found in the forms of  $\text{ClO}_3$  and  $\text{BrO}_3$ , and the coordinated oxygen atoms also adopt a lopsided mode in the known chlorates and bromates.<sup>24,25</sup> We have performed the quantum chemical calculations on the microscopic NLO properties of  $\text{ClO}_3$  and  $\text{BrO}_3$  using Gaussian09,<sup>26</sup> and the results are shown in Fig. 1. First, the HOMO–LUMO gaps of  $\text{ClO}_3$  and  $\text{BrO}_3$  are calculated to be 8.23 and 7.17 eV, respectively, which fall within the UV (even deep-UV) region and are comparable to those of  $\text{BO}_3$  and  $\text{CO}_3$  (especially for  $\text{ClO}_3$ ); moreover, due to the SCALP effect,  $\text{ClO}_3$  and  $\text{BrO}_3$  possess relatively large hyperpolarizabilities of 36.08 and 39.53 a.u., respectively, which are superior to  $\text{BO}_3$  and  $\text{CO}_3$  though inferior to  $\text{IO}_3$ . Meanwhile, their polarizability anisotropy is sufficiently large and comparable to that of  $\text{IO}_3$ , enabling them to achieve shorter-wavelength phase-matching SHG output. Therefore, given the favorable properties of the microscopic groups, chlorates and bromates have the potential to be UV (even short-wave UV and deep-UV) NLO candidates. However, few exploratory studies on the NLO properties of chlorates and bromates have been reported to date.<sup>27</sup>

In this work, the potential of chlorates and bromates as UV NLO materials is systematically explored for the first time. We search the Inorganic Crystal Structure Database (ICSD) for noncentrosymmetric ternary chlorates and bromates, excluding fluorides, transition metal and rare earth halates and nonstoichiometric compounds. Cubic symmetric compounds, such as  $\text{NaClO}_3$  and  $\text{NaBrO}_3$  ( $P2_13$ , No. 198), are also excluded because they cannot achieve phase-matching.<sup>28,29</sup> In this way, 15 cases of ternary main group chlorates and bromates are finally screened out and their NLO-related properties are carefully studied by first-principles methods. The results indicate that the halate crystals  $\text{AClO}_3$  and  $\text{ABrO}_3$  ( $A = \text{NH}_4, \text{K}, \text{Rb}$  and  $\text{Cs}$ ) with well-aligned motifs exhibit excellent UV NLO performance, including very short  $\lambda_{\text{PM}}$  deep into SWUV and DUV together with high SHG coefficients comparable to  $\beta\text{-BaB}_2\text{O}_4$ ,

being highlighted as important candidates for solar blind and even DUV NLO materials.

## Methods

The crystal structures of the halates are fully relaxed by employing the pseudopotential plane-wave method based on density functional theory within the total energy code of CASTEP.<sup>30–32</sup> Based on the optimized structures, the electronic structures and optical properties are also calculated. We choose the GGA-PBE functional and norm-conserving pseudopotential, in which  $\text{Cl}\text{-}3s^23p^5$ ,  $\text{O}\text{-}2s^22p^4$ ,  $\text{K}\text{-}3s^23p^64s^1$ ,  $\text{Rb}\text{-}4s^24p^65s^1$ ,  $\text{Cs}\text{-}5s^25p^66s^1$ ,  $\text{Sr}\text{-}4s^24p^65s^2$ ,  $\text{Ba}\text{-}5s^25p^66s^2$ ,  $\text{Tl}\text{-}5d^{10}6s^26p^1$ ,  $\text{Pb}\text{-}5s^25p^65d^{10}6s^26p^2$ ,  $\text{Bi}\text{-}5d^{10}6s^26p^3$ ,  $\text{N}\text{-}2s^22p^3$  and  $\text{H}\text{-}1s^1$  are considered as valence electrons.<sup>33,34</sup> The number of plane waves is determined by the cutoff energies of 820 and 750 eV for  $\text{Pb}(\text{ClO}_3)_2$  and other compounds, respectively, while the Monkhorst–Pack  $k$ -point separation is set to  $0.04 \text{ \AA}^{-1}$  to perform numerical integration of the Brillouin zone. During the optical property calculations, the number of empty bands is set to twice the number of valence bands to ensure convergence of refractive indices and SHG coefficients.

It is well known that DFT-GGA cannot accurately describe the eigenvalues of the electronic states, leading to a quantitative underestimation of the band gaps. Thus, the hybrid exchange and correlation functional of HSE06 is used to obtain more accurate band gaps.<sup>35</sup> When assessing the optical properties, the scissor operators (the gap differences between hybrid HSE06 and conventional GGA-PBE) are applied. This strategy has been demonstrated to be effective and reliable for the evaluation of optical properties of compounds without experimental band gaps.<sup>36</sup>

The NLO properties of the halates are calculated according to the full sum-over-states (SOS) formalism in the independent particle approximation,<sup>37,38</sup> and the static second-order NLO susceptibility can be expressed as<sup>39,40</sup>

$$\chi^{\alpha\beta\gamma} = \chi^{\alpha\beta\gamma}(\text{VE}) + \chi^{\alpha\beta\gamma}(\text{VH})$$

where  $\chi^{\alpha\beta\gamma}(\text{VE})$  and  $\chi^{\alpha\beta\gamma}(\text{VH})$  are the contributions to  $\chi^{\alpha\beta\gamma}$  from virtual-electron and virtual-hole processes, respectively, and can be given by

$$\begin{aligned} \chi_{\alpha\beta\gamma}^{(2)}(\text{VE}) &= \frac{e^3}{2\hbar^2 m^3} \sum_{vcc} \int \frac{d^3k}{4\pi^3} P(\alpha\beta\gamma) \text{Im} \left[ p_{cv}^\alpha p_{cc}^\beta p_{cv}^\gamma \right] \\ &\quad \times \left( \frac{1}{\omega_{cv}^3 \omega_{vc}^2} + \frac{2}{\omega_{vc}^4 \omega_{cv}^2} \right) \\ \chi_{\alpha\beta\gamma}^{(2)}(\text{VH}) &= \frac{e^3}{2\hbar^2 m^3} \sum_{v'v'c} \int \frac{d^3k}{4\pi^3} P(\alpha\beta\gamma) \text{Im} \left[ p_{v'v}^\alpha p_{v'c}^\beta p_{v'c}^\gamma \right] \\ &\quad \times \left( \frac{1}{\omega_{cv}^3 \omega_{v'c}^2} + \frac{2}{\omega_{vc}^4 \omega_{cv}^2} \right) \end{aligned}$$

Based on the SOS formalism, the “band-resolved”  $\chi^{(2)}$  can be readily given, and the relationship between each band/orbital and a specific SHG coefficient ( $d_{ij} = 1/2\chi^{(2)}$ ) can be con-

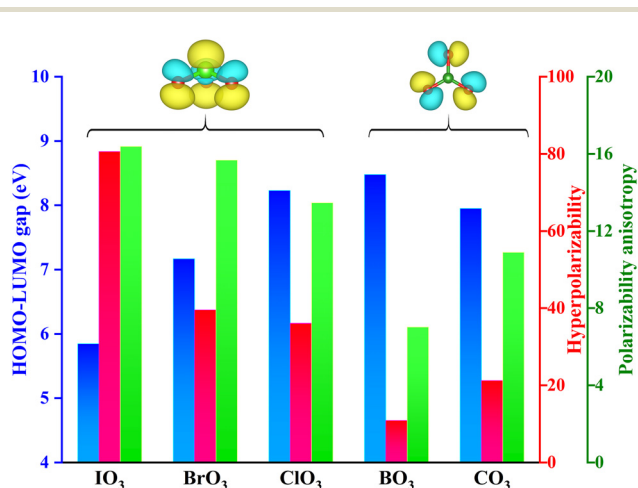


Fig. 1 Calculated HOMO–LUMO band gaps, hyperpolarizabilities and the polarizability anisotropy of  $\text{ClO}_3$  and  $\text{BrO}_3$  groups. The corresponding data of  $\text{BO}_3$ ,  $\text{CO}_3$  and  $\text{IO}_3$  are also calculated for comparison.

veniently established. Using the normalized SHG value of each band/orbital as the weighting coefficient, and summing all the SHG-weighted bands/orbitals in VB or CB over different  $k$ -points in space, the SHG-weighted electron density (SHG-density) can be obtained.<sup>41</sup> Through the “SHG-density” plots, the crystal orbitals that make significant contributions to the optical nonlinearity can be intuitively visualized.

In addition, to reveal the structural origin of birefringence, the polarizability anisotropy-weighted electron density [PAWED,  $\rho_{\Delta\chi}(r)$ ] has been defined.<sup>42</sup> It contains two parts of contributions (VB and CB) and can be formulated as

$$\rho_{\Delta\chi}^{\text{VB}}(r) = \sum_i^{\text{VB}} \omega_i |\psi_i(r)|^2$$

$$\rho_{\Delta\chi}^{\text{CB}}(r) = \sum_i^{\text{CB}} \omega_i |\psi_i(r)|^2$$

where  $|\psi_i(r)|^2$  is the electron density of the  $i$ th band/orbital; and  $\omega_i$  is the weighting factor describing the contribution ratio of the  $i$ th band/orbital to the total polarizability anisotropy ( $\Delta\chi^{(1)}$ ) of a crystal. In the low-frequency region,  $\omega_i$  can finally be quantified by the dielectric function  $\varepsilon$ ,

$$\omega_i = \frac{\Delta\chi_i^{(1)}}{\Delta\chi^{(1)}} = \frac{\varepsilon_i(\alpha\alpha) - \varepsilon_i(\beta\beta)}{\varepsilon(\alpha\alpha) - \varepsilon(\beta\beta)}$$

By utilizing the PAWED technique, the group/ion contributions to the birefringence (optical anisotropy) of compounds can be identified.<sup>43,44</sup>

## Results and discussion

### Crystal structures

Rigorous screening yields 15 cases of simple noncentrosymmetric chlorates and bromates, including  $\text{AClO}_3$  ( $A = \text{NH}_4, \text{K}, \text{Rb}, \text{Cs}, \text{Tl}$ ),  $\text{M}(\text{ClO}_3)_2$  ( $M = \text{Sr}, \text{Ba}, \text{Pb}$ ),  $\text{ABrO}_3$  ( $A = \text{K}, \text{Rb}, \text{Cs}, \text{Tl}$ ),  $\text{M}(\text{BrO}_3)_2$  ( $M = \text{Sr}, \text{Ba}$ ) and  $\text{BiO}(\text{BrO}_3)$ .<sup>24,25,45–50</sup> We have

performed the structural optimization on them, and the structural rationality is proved by the suitable bond valence sum of 4.8–5.2 for  $\text{Cl}^{5+}/\text{Br}^{5+}$  in  $\text{ClO}_3/\text{BrO}_3$  groups. They are all in the polar crystal symmetries and most of them with similar chemical formula are isostructural and the crystal structures resemble one another.

For the alkali metal/alkaline earth metal and  $\text{NH}_4$  halates, the anionic groups  $\text{ClO}_3/\text{BrO}_3$  are all isolated, so the geometric structures can be regarded as zero-dimensional.  $\text{AClO}_3$  and  $\text{ABrO}_3$  ( $A = \text{NH}_4, \text{K}, \text{Rb}, \text{Cs}, \text{Tl}$ ) are crystallized in the trigonal  $R3m$  space group (No. 160) and the  $\text{ClO}_3/\text{BrO}_3$  themselves have  $C3v$  symmetry with three identical  $\text{Cl-O}/\text{Br-O}$  bonds and all the isolated groups show perfect alignment with the dipoles pointing towards the crystallographic axis  $c$  (Fig. 2a).<sup>24,25,45–47</sup>  $\text{M}(\text{ClO}_3)_2$  and  $\text{M}(\text{BrO}_3)_2$  ( $M = \text{Sr}, \text{Ba}$ ) belong to the lower-symmetry monoclinic or orthorhombic crystal systems:  $\text{Sr}(\text{BrO}_3)_2$  crystallizes in the  $Cc$  space group (No. 9), while  $\text{Sr}(\text{ClO}_3)_2$ ,  $\text{Ba}(\text{ClO}_3)_2$  and  $\text{Ba}(\text{BrO}_3)_2$  are in the  $Fdd2$  space group (No. 43).<sup>48,49</sup> They are all characterized by distorted triangular pyramidal  $\text{ClO}_3/\text{BrO}_3$  and ionically bonded dodecahedral  $\text{MO}_8$ .

It is interesting that  $\text{Tl}^+$  also adopts a lopsided coordination style with three equivalent oxygen atoms in  $\text{TlClO}_3$  and  $\text{TlBrO}_3$  (Fig. 2b), but the stereochemical activity of the  $\text{Tl}^+ - 6s^2$  lone pair is to be investigated.  $\text{Pb}(\text{ClO}_3)_2$  is isostructural to  $\text{Sr}$  and  $\text{Ba}$  chlorates, and the  $\text{Pb}^{2+}$  cations are bisphenoidally coordinated with eight oxygen atoms from eight different  $\text{ClO}_3$ , forming dodecahedral geometries (Fig. 2c).<sup>49</sup> The stereochemical activity of the  $\text{Pb}^{2+} - 6s^2$  lone pairs is not obvious because the eight  $\text{Pb-O}$  bond lengths are relatively close, but this remains to be verified by electron localization function analysis.  $\text{BiO}(\text{BrO}_3)$  crystallizes in the polar space group  $Pca2_1$  (No. 29) and exhibits a layered structural topology with the  $\text{BrO}_3$  neatly hanging up and down from the infinite  $[\text{Bi}_2\text{O}_2]_\infty$  layers (Fig. 2d).<sup>50</sup>

### Nonlinear optics-related properties

For the noncentrosymmetric halates, we focus on their band gaps (UV transmittance), second-order nonlinear optical coefficients, birefringence (optical anisotropy) and phase-matching

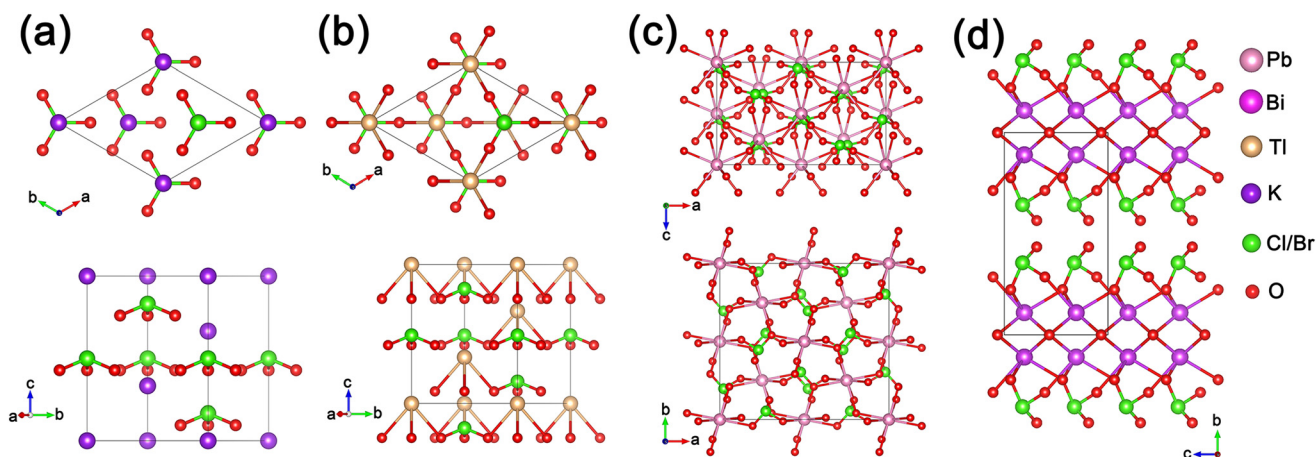


Fig. 2 Crystal structures of  $\text{KClO}_3$  (a),  $\text{TlClO}_3$  (b),  $\text{Pb}(\text{ClO}_3)_2$  (c) and  $\text{BiO}(\text{BrO}_3)$  (d).

properties, all of which are closely correlated to the practical applications of NLO materials. The calculated NLO-related property data of the halates are listed in Table 1, and  $\text{RbIO}_3$  and  $\text{CsIO}_3$  with available experimental/theoretical data are taken as references to check our computations. It is found that our calculated optical properties of  $\text{RbIO}_3$  and  $\text{CsIO}_3$  are in good agreement with the reported results, fully demonstrating the rationality and reliability of the calculation methods.

From the band structure data obtained by HSE06, we can see that there is an absolutely clear tendency for the band gaps of the halates being  $E_g(\text{chlorate}) > E_g(\text{bromate}) > E_g(\text{iodate})$  (Fig. S1,† Fig. 3a and Table 1), which is in agreement

with the results of the microscopic groups. The band gaps of alkali metal/alkaline earth metal chlorates are as wide as 6.8–7.0 eV, being comparable to or larger than those of some classical borates, such as  $\text{K}_2\text{Al}_2\text{B}_2\text{O}_7$  (6.89 eV),  $\text{CsLiB}_6\text{O}_{10}$  (6.89 eV),  $\text{Cs}_2\text{Al}_2(\text{B}_3\text{O}_6)_2\text{O}$  (7.05 eV),  $\text{Rb}_3\text{Ba}_3\text{Li}_2\text{Al}_4\text{B}_6\text{O}_{20}\text{F}$  (6.26 eV),  $\text{K}_3\text{Sr}_3\text{Li}_2\text{Al}_4\text{B}_6\text{O}_{20}\text{F}$  (6.53 eV),  $\text{LaBGeO}_5$  (6.40 eV), the well-known UV NLO crystal  $\beta\text{-BaB}_2\text{O}_4$  (6.43 eV), *etc.*<sup>51–56</sup> Hence, they are all deep-UV transparent, which is the most important requirement for DUV NLO materials. For alkali metal/alkaline earth metal bromates, the band gaps range from 5.65 to 6.18 eV, comparable to or larger than many carbonates, such as  $\text{ABCO}_3\text{F}$  (A = alkali metal, B = alkaline earth metal,  $\sim 6.20$  eV),

**Table 1** Space groups, calculated band gaps ( $E_g$ ) by hybrid HSE06, largest SHG coefficients ( $d_{ij}$ ), birefringence at 1064 nm ( $\Delta n$ ), UV cutoff wavelengths ( $\lambda_{\text{cutoff}}$ ), shortest phase-matching wavelengths ( $\lambda_{\text{PM}}$ ) and potential SHG applications for the halates

Material	Space group	$E_g$ (eV)	$d_{ij}$ ( $\text{pm V}^{-1}$ )	$\Delta n$	$\lambda_{\text{cutoff}}$ (nm)	$\lambda_{\text{PM}}$ (nm)	Potential SHG application
$(\text{NH}_4)(\text{ClO}_3)$	<i>R3m</i>	6.79	$d_{11} = 1.80$	0.168	182.6	194.9	DUV
$\text{KClO}_3$	<i>R3m</i>	6.86	$d_{11} = 1.85$	0.186	180.8	185.3	DUV
$\text{RbClO}_3$	<i>R3m</i>	6.81	$d_{11} = 1.88$	0.176	182.1	189.9	DUV
$\text{CsClO}_3$	<i>R3m</i>	6.99	$d_{11} = 1.63$	0.159	177.4	188.7	DUV
$\text{TlClO}_3$	<i>R3m</i>	5.23	$d_{11} = 2.37$	0.173	237.1	273.9	1064 $\rightarrow$ 532 nm
$\text{Sr}(\text{ClO}_3)_2$	<i>Fdd2</i>	7.03	$d_{24} = 1.23$	0.084	176.4	260.5	532 $\rightarrow$ 266 nm
$\text{Ba}(\text{ClO}_3)_2$	<i>Fdd2</i>	6.97	$d_{24} = 1.19$	0.089	177.9	255.7	532 $\rightarrow$ 266 nm
$\text{Pb}(\text{ClO}_3)_2$	<i>Fdd2</i>	5.62	$d_{24} = 2.37$	0.102	220.6	336.5	1064 $\rightarrow$ 532 nm
$\text{KBrO}_3$	<i>R3m</i>	5.65	$d_{11} = 2.76$	0.227	219.5	219.5	532 $\rightarrow$ 266 nm
$\text{RbBrO}_3$	<i>R3m</i>	5.77	$d_{11} = 2.61$	0.218	214.9	214.9	532 $\rightarrow$ 266 nm
$\text{CsBrO}_3$	<i>R3m</i>	5.90	$d_{11} = 2.39$	0.203	210.2	210.2	532 $\rightarrow$ 266 nm
$\text{TlBrO}_3$	<i>R3m</i>	5.00	$d_{11} = 3.19$	0.213	248.0	278.8	1064 $\rightarrow$ 532 nm
$\text{Sr}(\text{BrO}_3)_2$	<i>Cc</i>	6.14	$d_{26} = 1.64$	0.062	202.0	352.4	1064 $\rightarrow$ 532 nm
$\text{Ba}(\text{BrO}_3)_2$	<i>Fdd2</i>	6.18	$d_{24} = 1.80$	0.091	200.6	299.6	1064 $\rightarrow$ 532 nm
$\text{Bi}(\text{BrO}_3)_2$	<i>Pca2_1</i>	3.89	$d_{15} = 2.35$	0.040	318.8	815.5	NPM in UV-Vis SHG output
$\text{RbIO}_3$ <sup>16</sup>	<i>R3m</i>	4.06 4.0 <sup>a</sup>	$d_{31} = 3.08$ $20 \times \text{KDP}^a$	0.065 0.063 <sup>b</sup>	305.4	433.0	1064 $\rightarrow$ 532 nm
$\text{CsIO}_3$ <sup>17</sup>	<i>R3m</i>	4.38 4.2 <sup>a</sup>	$d_{31} = 1.99$ $15 \times \text{KDP}^a$	0.152 0.19 <sup>b</sup>	283.1	331.1	1064 $\rightarrow$ 532 nm

<sup>a</sup> Experimentally measured data in references. <sup>b</sup> Theoretically calculated data in references.

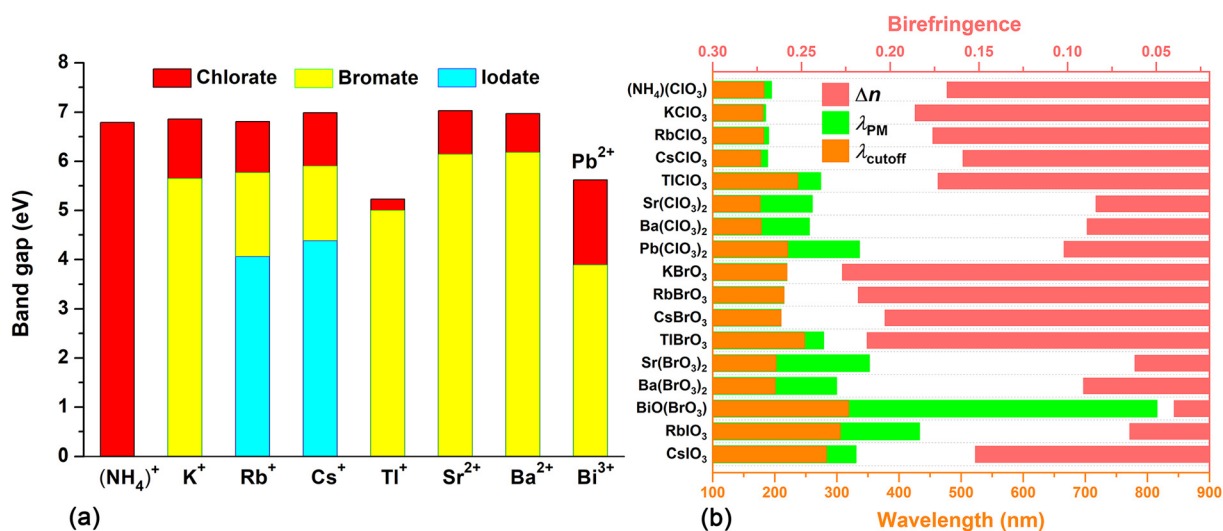


**Fig. 3** (a) Distribution of band gaps of the halates and (b) summarization of the birefringence, UV cutoff wavelengths ( $\lambda_{\text{cutoff}}$ ) and the shortest phase-matching wavelengths ( $\lambda_{\text{PM}}$ ) for the halates.

$\text{Cs}_3\text{Ba}_4(\text{CO}_3)_3\text{F}_5$  (5.90 eV),  $[\text{C}(\text{NH}_2)_3]_2\text{Zn}(\text{CO}_3)_2$  (5.90 eV),  $\text{Zn}(\text{NH}_3)_2\text{CO}_3$  (6.08 eV),  $\text{NaZnCO}_3\text{F}$  (4.61 eV),  $\text{Na}_4\text{Zn}(\text{CO}_3)_3$  (4.06 eV), *etc.*<sup>9,57–59</sup> Although the band gaps of the bromates are narrower than those of the corresponding chlorates by up to 0.79–1.21 eV, they still can be used as UV optical materials considering the good transparency in the short-wave UV region. It is worth noting that the Tl, Pb and Bi halates have much narrower band gaps than the alkali metal/alkaline earth metal halates, which is caused by the intrinsic intra-shell s–p transitions in the  $\text{Tl}^+$ ,  $\text{Pb}^{2+}$  and  $\text{Bi}^{3+}$  cations.

From Table 1, we can see that for the alkali metal and ammonium chlorates with *R3m* symmetry, the largest SHG tensor  $d_{11}$  values are 1.63–1.88  $\text{pm V}^{-1}$ , being up to 4.2–4.8 times that of KDP and 0.7–0.8 times that of  $\beta\text{-BaB}_2\text{O}_4$ , which have similar DUV transmittance to these chlorates. In comparison, the alkaline earth metal chlorates with *Fdd2* symmetry have relatively smaller SHG coefficients, where  $d_{24} = 1.23 \text{ pm V}^{-1}$  for  $\text{Sr}(\text{ClO}_3)_2$  and  $1.19 \text{ pm V}^{-1}$  for  $\text{Ba}(\text{ClO}_3)_2$ , but they are still 3 times larger than that of KDP and 0.5 times that of  $\beta\text{-BaB}_2\text{O}_4$ . Furthermore, the largest SHG tensors of  $\text{TlClO}_3$  ( $d_{11}$ ) and  $\text{Pb}(\text{ClO}_3)_2$  ( $d_{24}$ ) share the same value of  $2.37 \text{ pm V}^{-1}$  and are 6.1 times larger than that of KDP.

Not surprisingly, the SHG responses of the bromates are stronger than those of the corresponding chlorates, and there is a 35%–49% increase in SHG coefficients, resulting from the greater hyperpolarizability of  $\text{BrO}_3$  compared to  $\text{ClO}_3$ . Remarkably, the SHG effects of  $\text{ABrO}_3$  ( $A = \text{K, Rb, Cs}$ ;  $d_{11} = 2.39\text{--}2.76 \text{ pm V}^{-1} \approx 6.1\text{--}7.1 \times \text{KDP}$ ) are greater than those of many NLO carbonates and cyanurates with similar band gaps, such as  $\text{KCdCO}_3\text{F}$  (5.46 eV &  $5.2 \times \text{KDP}$ ),  $\text{KLi}(\text{HC}_3\text{N}_3\text{O}_3)\cdot 2\text{H}_2\text{O}$  (5.23 eV &  $5.3 \times \text{KDP}$ ),  $\text{Ln}_5(\text{C}_3\text{N}_3\text{O}_3)(\text{OH})_{12}$  ( $\text{Ln} = \text{Y, Lu}$ ; 5.28–5.51 eV &  $2.5\text{--}4.2 \times \text{KDP}$ ), *etc.*<sup>60–62</sup> Meanwhile,  $\text{Sr}(\text{BrO}_3)_2$  in *Cc* and  $\text{Ba}(\text{BrO}_3)_2$  in *Fdd2* show moderate SHG effects with the largest tensors being 1.64 and  $1.80 \text{ pm V}^{-1}$ , respectively. In addition,  $\text{TlBrO}_3$  exhibits the highest SHG effect among the bromates ( $d_{11} = 3.19 \text{ pm V}^{-1}$ ), which originates from its well-aligned motifs and smaller band gap. However, the SHG effect of  $\text{BiO}(\text{BrO}_3)$  with its very narrow band gap (3.89 eV &  $d_{15} = 2.35 \text{ pm V}^{-1}$ ) is weaker than those of the alkali metal bromates, which may be because the polarity of  $\text{BrO}_3$  is partially cancelled out in the compound.

The calculated refractive index results (Fig. S2† and Table 1) indicate that  $\text{AClO}_3$  and  $\text{ABrO}_3$  ( $A = \text{NH}_4, \text{K, Rb, Cs}$ ) in *R3m* possess very strong optical anisotropy and large birefringence (0.159–0.186 for  $\text{AClO}_3$  and 0.203–0.227 for  $\text{ABrO}_3$ ), enabling them to achieve phase-matching (PM) near their UV cutoff edges ( $\lambda_{\text{cutoff}}$ ; the deep-UV region for  $\text{AClO}_3$  and the short-wave UV region for  $\text{ABrO}_3$ ). In particular,  $\text{ABrO}_3$  crystals ( $A = \text{K, Rb}$  and  $\text{Cs}$ ) are even full-wavelength phase-matchable (FWPM) owing to their sufficiently large birefringence and small dispersion extent of their refractive index curves. In comparison, the alkaline earth metal halates in *Fdd2* and *Cc* show relatively small birefringence (0.062–0.091@1064 nm) and thus cannot achieve PM SHG output near their  $\lambda_{\text{cutoff}}$ . For example, although the  $\lambda_{\text{cutoff}}$  values of  $\text{Sr}(\text{ClO}_3)_2$  and  $\text{Ba}(\text{ClO}_3)_2$  are as short as 176.4 and 177.9 nm in the deep-UV region, their

shortest PM wavelengths ( $\lambda_{\text{PM}}$ ) are as long as 260.5 and 255.7 nm, implying that they can only output PM SHG light from 532 to 266 nm; so do  $\text{Sr}(\text{BrO}_3)_2$  and  $\text{Ba}(\text{BrO}_3)_2$ , which can only output PM SHG light from 1064 to 532 nm, despite their much shorter  $\lambda_{\text{cutoff}}$  values of 202.0 and 200.6 nm. It is worth noting that  $\text{BiO}(\text{BrO}_3)$  cannot realize phase-matching in the 1064 → 532 nm process due to its very small birefringence of 0.040@1064 nm. Interestingly, the birefringence  $\Delta n$ , the UV cutoff edges  $\lambda_{\text{cutoff}}$  and the shortest phase-matching wavelengths  $\lambda_{\text{PM}}$  of the halates are summarized in Fig. 3b, from which we can find the intrinsic relationship among the three optical indicators, *i.e.*, the larger the  $\Delta n$ , the closer the  $\lambda_{\text{PM}}$  is to  $\lambda_{\text{cutoff}}$ , even equalling  $\lambda_{\text{cutoff}}$ , namely the full-wavelength phase-matching (FWPM).<sup>11</sup>

Summarizing the above results, it is found that  $\text{AClO}_3$  ( $A = \text{NH}_4, \text{K, Rb, Cs}$ ) can be promising DUV NLO crystals with strong SHG responses; meanwhile,  $\text{M}(\text{ClO}_3)_2$  ( $M = \text{Sr, Ba}$ ) and  $\text{ABrO}_3$  ( $A = \text{K, Rb, Cs}$ ), particularly the latter with higher SHG effects and FWPM capability, can be important short-wave UV NLO materials capable of producing a 266 nm laser by SHG or quadruple frequency generation techniques. In addition,  $\text{TlClO}_3$ ,  $\text{Pb}(\text{ClO}_3)_2$ ,  $\text{TlBrO}_3$ ,  $\text{Sr}(\text{BrO}_3)_2$  and  $\text{Ba}(\text{BrO}_3)_2$  can also be potential SHG materials for application in the 1064 → 532 nm range of green light output.

### Structure–property relationship

For the screened NLO halates, the typical  $\text{KClO}_3$ ,  $\text{TlClO}_3$  and  $\text{Pb}(\text{ClO}_3)_2$  are taken as representatives to study their electronic structures and analyze the origin of their strong SHG effects and large birefringence. The effects of  $\text{Tl}^+$  and  $\text{Pb}^{2+}$  on the optical properties are also to be discussed.

From the partial density of states shown in Fig. 4a–c, it can be seen that there are fully overlapping electronic states between Cl and O in the VB range of  $-12\text{--}5 \text{ eV}$  and in the CB range of  $5\text{--}10 \text{ eV}$ , indicating the strong covalent interactions of Cl–O bonds in the halates. K-3p, Tl-5d and Pb-5d are highly localized in the deep energy levels ( $< -8 \text{ eV}$ ), so they would have little effect on the optical properties. For  $\text{KClO}_3$ , the upper part of VB is dominated by the O-2p nonbonding states, mixed with a few Cl-3s3p nonbonding states, and the lower part of CB consists of the unoccupied O-2p and Cl-3p orbitals, so the wide band gap of  $\text{KClO}_3$  is determined by the  $\text{ClO}_3$  groups. The electronic structures of  $\text{TlClO}_3$  and  $\text{Pb}(\text{ClO}_3)_2$  are more complicated: except for the usual O-2p and Cl-3s3p, Tl-6s6p and Pb-6s6p are also involved in the VB top and CB bottom, so their band gaps are determined by  $\text{ClO}_3$  together with the  $\text{Tl}^+/\text{Pb}^{2+}$  cations. Considering the much narrower band gaps of  $\text{TlClO}_3$  and  $\text{Pb}(\text{ClO}_3)_2$  compared to that of  $\text{KClO}_3$ , it can be confirmed that  $\text{Tl}^+/\text{Pb}^{2+}$  has a weakening effect on the band gaps of the compounds. To further investigate the stereoactivity of the lone pair electrons ( $6s^2$ ) on the  $\text{Tl}^+$  and  $\text{Pb}^{2+}$  cations, the electron localization functions (ELFs) of  $\text{TlClO}_3$  and  $\text{Pb}(\text{ClO}_3)_2$  are calculated and plotted with  $\eta = 0.9$  (Fig. S3†). It clearly shows that there are lobe-like isosurfaces on the  $\text{Cl}^{5+}$  ions in both compounds, confirming the highly stereoactive  $\text{Cl}^{5+}\text{-}3s^2$  lone pair, whereas the isosurfaces around

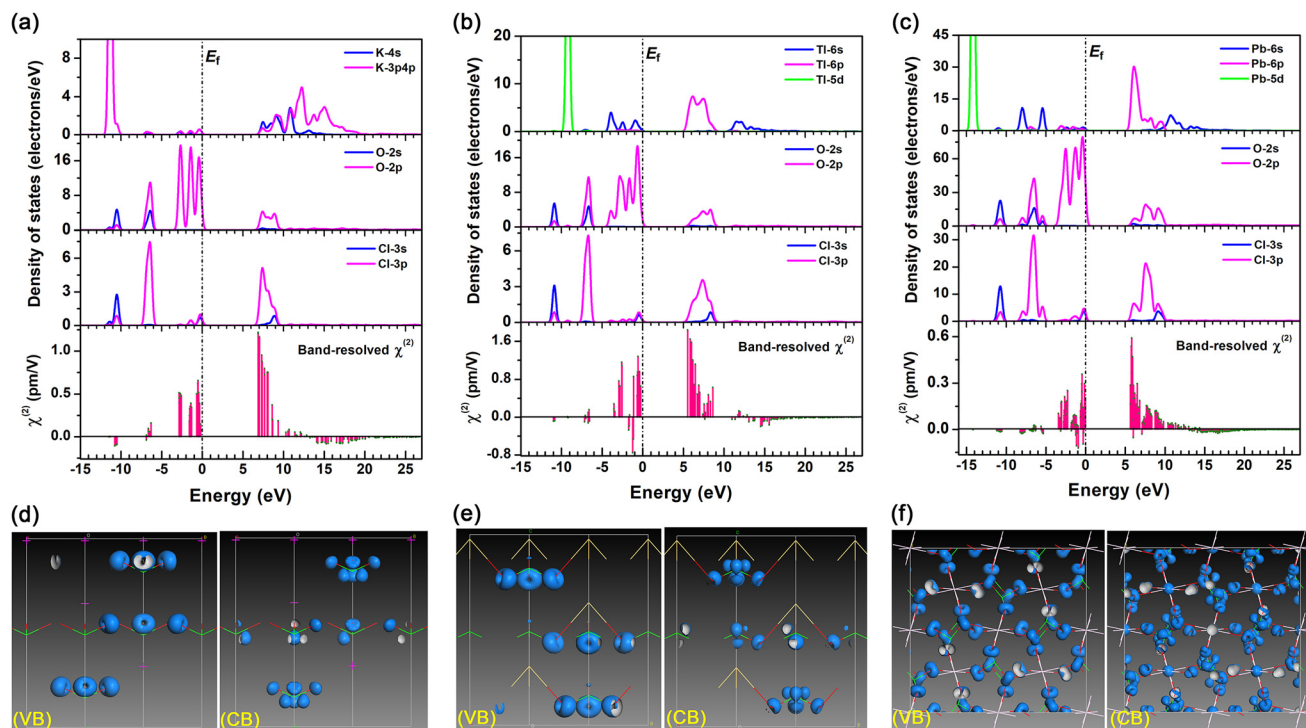


**Fig. 4** Partial density of states and band-resolved NLO susceptibility  $\chi^{(2)}$  (a–c) and SHG-density plots (d–f) for  $\text{KClO}_3$ ,  $\text{TlClO}_3$  and  $\text{Pb}(\text{ClO}_3)_2$ , respectively.

$\text{Tl}^+$  and  $\text{Pb}^{2+}$  (especially  $\text{Pb}^{2+}$ ) are nearly spherical, indicating that the  $\text{Tl}^+-6s^2$  and  $\text{Pb}^{2+}-6s^2$  lone pair electrons are much less stereoactive and almost inert.

Band-resolved  $\chi^{(2)}$  and SHG-density techniques are used to explore the origin of the strong SHG effects for these simple halates. The former can help us to know which energy levels give large contributions to SHG, and the latter can intuitively show the specific SHG-contributing orbitals and atoms in real space. From the band-resolved  $\chi^{(2)}$  in the bottom panels of the DOS graphs (Fig. 4a–c), we can see that the states distributed on both sides of their forbidden bands ( $-4$ – $0$  eV and  $5$ – $10$  eV) give the majority of the SHG contributions, corresponding to O-2p nonbonding states and a small amount of Cl-3s3p, Tl-6s and Pb-6s6p states in VB and the empty orbitals of Cl-3p, O-2p, K-4s4p, Tl-6p and Pb-6p in CB. The SHG-density graphs (Fig. 4d–f) for the three compounds indicate that not all of the above electronic states are involved in contributing to the SHG process. In fact, only the nonbonding states of O-2p in VB and the unoccupied Cl-3p, O-2p and a few Pb-6p orbitals in CB make real contributions to the strong NLO responses of  $\text{KClO}_3$ ,  $\text{TlClO}_3$  and  $\text{Pb}(\text{ClO}_3)_2$ . Furthermore, based on the SHG-density data, the contribution percentages of all groups and ions can be obtained (Table 2); apart from the core  $\text{ClO}_3$  groups, which play an overwhelming role in the SHG effects,  $\text{TlO}_3$  and  $\text{PbO}_8$  groups also make some contributions, 29.37% and 26.17% respectively, while the contributions from  $\text{K}^+$  are negligible.

In addition, we use the polarizability anisotropy-weighted electron density (PAWED) method to investigate the structural source of the large birefringence of these compounds

**Table 2** Calculated contribution percentages of different groups to SHG coefficients and the birefringence for  $\text{KClO}_3$ ,  $\text{TlClO}_3$  and  $\text{Pb}(\text{ClO}_3)_2$

Material	Group	$d_{ij}$ ( $\text{pm V}^{-1}$ )	$\Delta n$
$\text{KClO}_3$	$\text{ClO}_3$ $\text{K}^+$	$d_{11} = 1.85$	0.186
		98.46%	96.78%
		1.53%	3.18%
$\text{TlClO}_3$	$\text{ClO}_3$ $\text{TlO}_3$	$d_{11} = 2.37$	0.173
		70.63%	74.00%
		29.37%	25.96%
$\text{Pb}(\text{ClO}_3)_2$	$\text{ClO}_3$ $\text{PbO}_8$	$d_{24} = 2.37$	0.102
		72.31%	73.22%
		26.17%	25.40%

(Fig. S4<sup>†</sup>). In VB, the birefringence originates from the O-2p nonbonding states, and in CB, it is mainly from the Cl-3p and O-2p, mixed with some Pb-6p empty orbitals. The calculated contribution values (Table 2) are similar to those obtained for SHG effects:  $\text{ClO}_3$  groups also play a predominant role in generating large birefringence, while the contributions from  $\text{TlO}_3$  and  $\text{PbO}_8$  groups are not very large, which can be attributed to the almost inert stereoactivity of the  $6s^2$  lone pairs on the  $\text{Tl}^+$  and  $\text{Pb}^{2+}$  cations.

## Conclusions

In summary, the long-neglected stereochemically active lone pair (SCALP) groups  $\text{ClO}_3$  and  $\text{BrO}_3$  are innovatively proposed to be good UV NLO functional motifs based on the group prop-

erty prediction, and the NLO performance of chlorates and bromates is firstly investigated systematically by employing the density functional theory method within the CASTEP code. Through careful compound screening, structural optimization, property simulation and mechanism analysis, the halate crystals  $\text{AClO}_3$  and  $\text{ABrO}_3$  ( $A = \text{NH}_4, \text{K}, \text{Rb}$  and  $\text{Cs}$ ) with well-arranged SCALP motifs are highlighted as promising UV NLO materials in view of their excellent properties, including wide UV transparent ranges deep into DUV for chlorates and SWUV for bromates, high SHG effects comparable to  $\beta\text{-BaB}_2\text{O}_4$ , large birefringence and strong phase-matching ability. Concretely,  $\text{AClO}_3$  crystals can be potential DUV NLO candidates ( $4.2\text{--}4.8 \times \text{KDP}$  &  $\lambda_{\text{PM}} = 185\text{--}195 \text{ nm}$ ), and  $\text{ABrO}_3$  crystals, showing very strong SHG responses ( $6.1\text{--}7.1 \times \text{KDP}$ ) and rare full-wavelength phase-matching capability ( $\lambda_{\text{PM}} = \lambda_{\text{cutoff}} = 210\text{--}220 \text{ nm}$ ), can be important short-wave UV NLO materials. Hence the UV NLO potential of  $\text{ClO}_3$  and  $\text{BrO}_3$  is fully demonstrated, and this work provides novel functional motifs and opens up a new avenue for the development of SWUV and even DUV NLO materials.

## Author contributions

Chun-Li Hu performed the theoretical calculations, data analyses, and paper writing. Qian-Qian Chen and Fang Kong performed crystal structure screening. Jiang-Gao Mao provided data analyses and major revisions of the manuscript. All the authors discussed the results and commented on the manuscript.

## Conflicts of interest

There are no conflicts to declare.

## Acknowledgements

This work was financially supported by the National Natural Science Foundation of China (Grant No. 22375201, 22031009 and 21921001) and Fujian Science & Technology Innovation Laboratory for Optoelectronic Information of China (2021ZR121).

## References

- M. Mutailipu, F. M. Li, C. C. Jin, Z. H. Yang, K. R. Poeppelmeier and S. L. Pan, Strong Nonlinearity Induced by Coaxial Alignment of Polar Chain and Dense  $[\text{BO}_3]$  Units in  $\text{CaZn}_2(\text{BO}_3)_2$ , *Angew. Chem., Int. Ed.*, 2022, **61**(21), e202202096.
- P. Becker, Borate Materials in Nonlinear Optics, *Adv. Mater.*, 1998, **10**, 979–992.
- H. Xuan, H. Igarashi, S. Ito, C. Qu, Z. Zhao and Y. Kobayashi, High-Power, Solid-State, Deep Ultraviolet Laser Generation, *Appl. Sci.*, 2018, **8**(2), 233.
- R. Jiang, D. Mou, Y. Wu, L. Huang, C. D. McMillen, J. Kolis, H. G. Giesber, J. J. Egan and A. Kaminski, Tunable vacuum ultraviolet laser based spectrometer for angle resolved photoemission spectroscopy, *Rev. Sci. Instrum.*, 2014, **85**(3), 033902.
- C. Chen, T. Sasaki, R. Li, Y. Wu, Z. Lin, Y. Mori, Z. Hu, J. Wang, S. Uda, M. Yoshimura and Y. Kaneda, *Nonlinear Optical Borate Crystals: Principles and Applications*. Wiley-VCH, Weinheim, Germany, 2012.
- P. S. Halasyamani and K. R. Poeppelmeier, Noncentrosymmetric Oxides, *Chem. Mater.*, 1998, **10**, 2753–2769.
- W. Zhou and S. P. Guo, Rational Design of Novel Promising Infrared Nonlinear Optical Materials: Structural Chemistry and Balanced Performances, *Acc. Chem. Res.*, 2024, **57**, 648–660.
- Y. N. Xia, C. T. Chen, D. Y. Tang and B. C. Wu, New Nonlinear Optical Crystals for UV and VUV Harmonic Generation, *Adv. Mater.*, 1995, **7**, 79–81.
- G. Zou, N. Ye, L. Huang and X. Lin, Alkaline-Alkaline Earth Fluoride Carbonate Crystals  $\text{ABCO}_3\text{F}$  ( $A = \text{K}, \text{Rb}, \text{Cs}; B = \text{Ca}, \text{Sr}, \text{Ba}$ ) as Nonlinear Optical Materials, *J. Am. Chem. Soc.*, 2011, **133**(49), 20001–20007.
- X. Wang, Y. Wang, B. Zhang, F. Zhang, Z. Yang and S. Pan,  $\text{CsB}_4\text{O}_6\text{F}$ : A Congruent-Melting Deep-Ultraviolet Nonlinear Optical Material by Combining Superior Functional Units, *Angew. Chem., Int. Ed.*, 2017, **56**, 14119–14123.
- M. Mutailipu, J. Han, Z. Li, F. Li, J. Li, F. Zhang, X. Long, Z. Yang and S. Pan, Achieving the full-wavelength phase-matching for efficient nonlinear optical frequency conversion in  $\text{C}(\text{NH}_2)_3\text{BF}_4$ , *Nat. Photonics*, 2023, **17**(8), 694–701.
- J. Lu, J.-N. Yue, L. Xiong, W.-K. Zhang, L. Chen and L.-M. Wu, Uniform Alignment of Non- $\pi$ -Conjugated Species Enhances Deep Ultraviolet Optical Nonlinearity, *J. Am. Chem. Soc.*, 2019, **141**(20), 8093–8097.
- C.-L. Hu and J.-G. Mao, Recent advances on second-order NLO materials based on metal iodates, *Coord. Chem. Rev.*, 2015, **288**, 1–17.
- M. Gai, T. Tong, Y. Wang, Z. Yang and S. Pan, New Alkaline-Earth Metal Fluoroiodates Exhibiting Large Birefringence and Short Ultraviolet Cutoff Edge with Highly Polarizable  $(\text{IO}_3\text{F})^{2-}$  Units, *Chem. Mater.*, 2020, **32**(13), 5723–5728.
- F. R. Nash, J. G. Bergman, G. D. Boyd and E. H. Turner, Optical Nonlinearities in  $\text{LiIO}_3$ , *J. Appl. Phys.*, 1969, **40**(13), 5201–5206.
- Q. Wu, H. Liu, F. Jiang, L. Kang, L. Yang, Z. Lin, Z. Hu, X. Chen, X. Meng and J. Qin,  $\text{RbIO}_3$  and  $\text{RbIO}_2\text{F}_2$ : Two Promising Nonlinear Optical Materials in Mid-IR Region and Influence of Partially Replacing Oxygen with Fluorine for Improving Laser Damage Threshold, *Chem. Mater.*, 2016, **28**(5), 1413–1418.
- M. Zhang, C. Hu, T. Abudouwufu, Z. Yang and S. Pan, Functional Materials Design via Structural Regulation

- Originated from Ions Introduction: A Study Case in Cesium Iodate System, *Chem. Mater.*, 2018, **30**(3), 1136–1145.
- 18 F.-F. Mao, C.-L. Hu, J. Chen and J.-G. Mao, A Series of Mixed-Metal Germanium Iodates as Second-Order Nonlinear Optical Materials, *Chem. Mater.*, 2018, **30**(7), 2443–2452.
  - 19 Y. H. Kim, T. T. Tran, P. S. Halasyamani and K. M. Ok, Macroscopic polarity control with alkali metal cation size and coordination environment in a series of tin iodates, *Inorg. Chem. Front.*, 2015, **2**(4), 361–368.
  - 20 H.-Y. Chang, S.-H. Kim, P. S. Halasyamani and K. M. Ok, Alignment of Lone Pairs in a New Polar Material: Synthesis, Characterization, and Functional Properties of  $\text{Li}_2\text{Ti}(\text{IO}_3)_6$ , *J. Am. Chem. Soc.*, 2009, **131**(7), 2426–2427.
  - 21 M.-L. Liang, C.-L. Hu, F. Kong and J.-G. Mao, BiFSeO<sub>3</sub>: An Excellent SHG Material Designed by Aliovalent Substitution, *J. Am. Chem. Soc.*, 2016, **138**(30), 9433–9436.
  - 22 Y.-J. Jia, X. Zhang, Y.-G. Chen, X. Jiang, J.-N. Song, Z. Lin and X.-M. Zhang,  $\text{PbBi}(\text{SeO}_3)_2\text{F}$  and  $\text{Pb}_2\text{Bi}(\text{SeO}_3)_2\text{Cl}_3$ : Coexistence of Three Kinds of Stereochemically Active Lone-Pair Cations Exhibiting Excellent Nonlinear Optical Properties, *Inorg. Chem.*, 2022, **61**(39), 15368–15376.
  - 23 R. Robert, V. Balisetty, K. Mohanrao, M. M. Pappan, S. Mangalassery, D. N. Rao and K. Vidyasagar, Syntheses, Crystal Structure, and Second Harmonic Generation Response of Noncentrosymmetric Layered Selenites and Tellurites of Antimony(V),  $\text{ASb}_3\text{X}_2\text{O}_{12}$  (A = K, Rb, Cs, Tl; X = Se, Te), *Inorg. Chem.*, 2023, **62**(20), 7890–7897.
  - 24 C. W. F. T. Pistorius, Lattice Constants of the High-Pressure Phase  $\text{KClO}_3$  II, *J. Chem. Phys.*, 1972, **56**(12), 6263–6264.
  - 25 M. Szafranski and K. Ståhl, Refinements of the crystal structures and UV-absorption properties of  $\text{KBrO}_3$ ,  $\text{RbBrO}_3$  and  $\text{CsBrO}_3$ , *Z. Kristallogr. – Cryst. Mater.*, 1994, **209**(6), 491–494.
  - 26 M. J. Frisch, G. Trucks, H. Schlegel, G. Scuseria, M. Robb, J. Cheeseman, G. Scalmani, V. Barone, B. Mennucci and G. Petersson, *Gaussian 09, Revision D. 01*. Gaussian, Inc., Wallingford, CT, 2009.
  - 27 F. Kong, C.-L. Hu, M.-L. Liang and J.-G. Mao,  $\text{Pb}_4(\text{OH})_4(\text{BrO}_3)_3(\text{NO}_3)$ : An Example of SHG Crystal in Metal Bromates Containing  $\pi$ -Conjugated Planar Triangle, *Inorg. Chem.*, 2015, **55**(2), 948–955.
  - 28 M. E. Burke-Laing and K. N. Trueblood, Sodium chlorate: precise dimensions for the  $\text{ClO}_3^-$  ion, *Acta Crystallogr., Sect. B: Struct. Crystallogr. Cryst. Chem.*, 1977, **33**(8), 2698–2699.
  - 29 S. C. Abrahams and J. L. Bernstein, Remeasurement of optically active  $\text{NaClO}_3$  and  $\text{NaBrO}_3$ , *Acta Crystallogr., Sect. B: Struct. Crystallogr. Cryst. Chem.*, 1977, **33**(11), 3601–3604.
  - 30 S. J. Clark, M. D. Segall, C. J. Pickard, P. J. Hasnip, M. I. J. Probert, K. Refson and M. C. Payne, First principles methods using CASTEP, *Z. Kristallogr.*, 2005, **220**(5/6), 567–570.
  - 31 M. D. Segall, P. J. D. Lindan, M. J. Probert, C. J. Pickard, P. J. Hasnip, S. J. Clark and M. C. Payne, First-principles simulation: ideas, illustrations and the CASTEP code, *J. Phys.: Condens. Matter*, 2002, **14**(11), 2717–2744.
  - 32 V. Milman, B. Winkler, J. A. White, C. J. Pickard, M. C. Payne, E. V. Akhmatkaya and R. H. Nobes, Electronic structure, properties, and phase stability of inorganic crystals: A pseudopotential plane-wave study, *Int. J. Quantum Chem.*, 2000, **77**(5), 895–910.
  - 33 J. P. Perdew, K. Burke and M. Ernzerhof, Generalized Gradient Approximation Made Simple, *Phys. Rev. Lett.*, 1996, **77**(18), 3865–3868.
  - 34 J. S. Lin, A. Qteish, M. C. Payne and V. V. Heine, Optimized and transferable nonlocal separable ab initio pseudopotentials, *Phys. Rev. B: Condens. Matter Mater. Phys.*, 1993, **47**(8), 4174–4180.
  - 35 A. V. Krukau, O. A. Vydrov, A. F. Izmaylov and G. E. Scuseria, Influence of the exchange screening parameter on the performance of screened hybrid functionals, *J. Chem. Phys.*, 2006, **125**(22), 224106.
  - 36 Z. S. Lin, L. Kang, T. Zheng, R. He, H. Huang and C. T. Chen, Strategy for the optical property studies in ultraviolet nonlinear optical crystals from density functional theory, *Comput. Mater. Sci.*, 2012, **60**, 99–104.
  - 37 S. N. Rashkeev, W. R. L. Lambrecht and B. Segall, Efficient ab initio method for the calculation of frequency-dependent second-order optical response in semiconductors, *Phys. Rev. B: Condens. Matter Mater. Phys.*, 1998, **57**(7), 3905–3919.
  - 38 C. Aversa and J. E. Sipe, Nonlinear optical susceptibilities of semiconductors: Results with a length-gauge analysis, *Phys. Rev. B: Condens. Matter Mater. Phys.*, 1995, **52**(20), 14636–14645.
  - 39 J. Lin, M.-H. Lee, Z.-P. Liu, C. Chen and C. J. Pickard, Mechanism for linear and nonlinear optical effects in  $\beta$ - $\text{BaB}_2\text{O}_4$  crystals, *Phys. Rev. B: Condens. Matter Mater. Phys.*, 1999, **60**(19), 13380–13389.
  - 40 B. Zhang, M.-H. Lee, Z. Yang, Q. Jing, S. Pan, M. Zhang, H. Wu, X. Su and C.-S. Li, Simulated pressure-induced blue-shift of phase-matching region and nonlinear optical mechanism for  $\text{K}_3\text{B}_6\text{O}_{10}\text{X}$  (X = Cl, Br), *Appl. Phys. Lett.*, 2015, **106**(3), 031906.
  - 41 C.-H. Lo and M.-H. Lee, *The Role of Electron Lone-pair in the Optical Nonlinearity of Oxide, Nitride and Halide Crystals*. Master, Tamkang University, Taiwan, 2005.
  - 42 C.-L. Hu, J. Chen, Z. Fang, R.-L. Tang and J.-G. Mao,  $\text{LiB}_2\text{O}_3\text{F}$ : A Beryllium-Free Deep-Ultraviolet Nonlinear Optical Material Designed Based on a Boron-Rich Strategy, *Chem. Mater.*, 2021, **33**(12), 4783–4791.
  - 43 R.-L. Tang, W. Xu, W.-J. Xie; and C.-L. Hu,  $\text{Sc}_2\text{F}_2(\text{B}_2\text{O}_5)$ : a deep ultraviolet scandium borate fluoride exhibiting large birefringence induced by the synergistic effect of  $\text{B}_2\text{O}_5$  and  $\text{ScO}_n\text{F}_2$  groups, *Inorg. Chem. Front.*, 2022, **9**(20), 5153–5160.
  - 44 C.-L. Hu, Y.-X. Han, Z. Fang and J.-G. Mao,  $\text{Zn}_2\text{BS}_3\text{Br}$ : An Infrared Nonlinear Optical Material with Significant Dual-Property Enhancements Designed through a Template Grafting Strategy, *Chem. Mater.*, 2023, **35**(6), 2647–2654.
  - 45 G. Brunton, The absolute configuration of  $\text{RbClO}_3$ , *Mater. Res. Bull.*, 1973, **8**(7), 791–793.

- 46 S. D. Griesemer, L. Ward and C. Wolverton, High-throughput crystal structure solution using prototypes, *Phys. Rev. Mater.*, 2021, **5**(10), 105003.
- 47 R. B. Gillespie, P. K. Gantzel and K. N. Trueblood, The crystal structure of ammonium chlorate, *Acta Crystallogr.*, 1962, **15**(12), 1271–1272.
- 48 H. D. Lutz, W. Buchmeier, E. Alici and W. Eckers, Röntgenographische und schwingungsspektroskopische Untersuchungen an wasserfreien Chloraten und Bromaten des Strontiums, Bariums und Bleis. Kristallstruktur des  $\text{Sr}(\text{ClO}_3)_2$  und  $\text{Sr}(\text{BrO}_3)_2$ , *Z. Anorg. Allg. Chem.*, 2004, **529**(10), 46–56.
- 49 H. D. Lutz, W. Buchmeier, M. Jung and T. Kellersohn, A comparative study of the crystal structures of  $\text{Ba}(\text{ClO}_3)_2$ ,  $\text{Ba}(\text{BrO}_3)_2$  II,  $\text{Pb}(\text{ClO}_3)_2$ , and  $\text{Sr}(\text{ClO}_3)_2$ , *Z. Kristallogr. – Cryst. Mater.*, 1989, **189**(1–4), 131–140.
- 50 X.-D. Dong, Y.-M. Zhang and Z.-Y. Zhao, Role of the Polar Electric Field in Bismuth Oxyhalides for Photocatalytic Water Splitting, *Inorg. Chem.*, 2021, **60**(12), 8461–8474.
- 51 N. Ye, W. Zeng, J. Jiang, B. Wu, C. Chen, B. Feng and X. Zhang, New nonlinear optical crystal  $\text{K}_2\text{Al}_2\text{B}_2\text{O}_7$ , *J. Opt. Soc. Am. B*, 2000, **17**(5), 764–768.
- 52 L. Li, Q. Jing, Z. Yang, X. Su, B.-H. Lei, S. Pan, F. Zhang and J. Zhang, Effect of the tetrahedral groups on the optical properties of  $\text{LaBRO}_3$  (R = Si and Ge): A first-principles study, *J. Appl. Phys.*, 2015, **118**(11), 113104.
- 53 H. Wu, H. Yu, S. Pan and P. S. Halasyamani, Deep-Ultraviolet Nonlinear-Optical Material  $\text{K}_3\text{Sr}_3\text{Li}_2\text{Al}_4\text{B}_6\text{O}_{20}\text{F}$ : Addressing the Structural Instability Problem in  $\text{KBe}_2\text{BO}_3\text{F}_2$ , *Inorg. Chem.*, 2017, **56**(15), 8755–8758.
- 54 Z. Fang, X. Jiang, M. Duan, Z. Hou, C. Tang, M. Xia, L. Liu, Z. Lin, F. Fan, L. Bai and C. Chen, Deep-Ultraviolet Nonlinear Optical Crystal  $\text{Cs}_2\text{Al}_2(\text{B}_3\text{O}_6)_2\text{O}$ : A Benign Member of the  $\text{Sr}_2\text{Be}_2(\text{BO}_3)_2\text{O}$  Family with  $[\text{Al}_2(\text{B}_3\text{O}_6)_2\text{O}]^{2-}$  Double Layers, *Chem. – Eur. J.*, 2018, **24**(31), 7856–7860.
- 55 H. Yu, J. Young, H. Wu, W. Zhang, J. M. Rondinelli and S. Halasyamani, The Next-Generation of Nonlinear Optical Materials:  $\text{Rb}_3\text{Ba}_3\text{Li}_2\text{Al}_4\text{B}_6\text{O}_{20}\text{F}$ —Synthesis, Characterization, and Crystal Growth, *Adv. Opt. Mater.*, 2017, **5**(23), 1700840.
- 56 D. N. Nikogosyan, *Nonlinear Optical Crystals, A Complete Survey*. Springer, New York, 2005.
- 57 H.-X. Tang, Q.-R. Shui, R.-B. Fu, Z.-Q. Zhou, W.-X. Bao, Z.-J. Ma and X.-T. Wu,  $\text{Zn}(\text{NH}_3)\text{CO}_3$ : a “three-in-one” UV nonlinear optical crystal built by a polar molecule bonding strategy, *J. Mater. Chem. C*, 2021, **9**(46), 16477–16484.
- 58 G. Peng, Y.-H. Tang, C. Lin, D. Zhao, M. Luo, T. Yan, Y. Chen and N. Ye, Exploration of new UV nonlinear optical materials in the sodium–zinc fluoride carbonate system with the discovery of a new regulation mechanism for the arrangement of  $[\text{CO}_3]^{2-}$  groups, *J. Mater. Chem. C*, 2018, **6**(24), 6526–6533.
- 59 Z. Bai, L. Liu, Z. Lin and K. M. Ok,  $[\text{C}(\text{NH}_2)_3]_2\text{Zn}(\text{CO}_3)_2$ : A Guanidinium-Templated Ultraviolet Nonlinear Optical Material, *Inorg. Chem.*, 2022, **61**(31), 12473–12480.
- 60 D. Lin, M. Luo, C. Lin, F. Xu and N. Ye,  $\text{KLi}(\text{HC}_3\text{N}_3\text{O}_3)\cdot 2\text{H}_2\text{O}$ : Solvent-drop Grinding Method toward the Hydro-isocyanurate Nonlinear Optical Crystal, *J. Am. Chem. Soc.*, 2019, **141**(8), 3390–3394.
- 61 Y. Lin, C.-L. Hu and J.-G. Mao,  $\text{K}_2\text{Pb}_3(\text{CO}_3)_3\text{F}_2$  and  $\text{KCdCO}_3\text{F}$ : Novel Fluoride Carbonates with Layered and 3D Framework Structures, *Inorg. Chem.*, 2015, **54**(21), 10407–10414.
- 62 X. Meng, X. Zhang, Q. Liu, Z. Zhou, X. Jiang, Y. Wang, Z. Lin and M. Xia, Perfectly Encoding  $\pi$ -Conjugated Anions in the  $\text{RE}_5(\text{C}_3\text{N}_3\text{O}_3)(\text{OH})_{12}$  (RE=Y, Yb, Lu) Family with Strong Second Harmonic Generation Response and Balanced Birefringence, *Angew. Chem., Int. Ed.*, 2023, **62**(1), e202214848.